Cancer Letters 457 (2019) 110–118

Contents lists available at ScienceDirect

Cancer Letters

journal homepage: www.elsevier.com/locate/canlet

Original Articles

Porphyrin-lipid assemblies and nanovesicles overcome ABC transporter-mediated photodynamic therapy resistance in cancer cells

Yan Baglo[a], Barry J. Liang[a], Robert W. Robey[b], Suresh V. Ambudkar[b], Michael M. Gottesman[b], Huang-Chiao Huang[a,c,d,*]

[a] Fischell Department of Bioengineering, University of Maryland, College Park, MD, 20742, USA
[b] Laboratory of Cell Biology, National Cancer Institute, National Institutes of Health, Bethesda, MD, 20892, USA
[c] Marlene and Stewart Greenebaum Cancer Center, University of Maryland School of Medicine, Baltimore, MD, 21201, USA
[d] Wellman Center for Photomedicine, Massachusetts General Hospital, Boston, MA, 02114, USA

ARTICLE INFO

Keywords:
Multidrug resistance
ATP-binding cassette transporters
Benzoporphyrin derivative
Porphysome nanotechnology
Photodynamic therapy

ABSTRACT

Photodynamic therapy (PDT) involves light activation of the photosensitizer to generate reactive molecular species that induce cell modulation or death. Based on earlier findings showing that the photosensitizer benzoporphyrin derivative (BPD) is a breast cancer resistance protein (ABCG2) substrate, we investigated the ability of the P-glycoprotein (P-gp) and multidrug resistance-associated protein 1 (MRP1) to transport BPD. In a panel of breast cancer cell lines overexpressing P-gp, MRP1, or ABCG2, BPD transport occurs only in cells overexpressing P-gp and ABCG2. Intracellular BPD fluorescence is not affected by MRP1, as determined by flow cytometry. To bypass P-gp- and ABCG2-mediated efflux of BPD, we introduce a lipidation strategy to create BPD derivatives that are no longer P-gp and ABCG2 substrates. The phospholipid-conjugated BPD and its nanoliposomal formulation evade both P-gp- and ABCG2-mediated transport. In cytotoxicity assays, lipidated BPD and its nanoliposomal formulation abrogate P-gp- and ABCG2-mediated PDT resistance. We verify that P-gp, like ABCG2, plays a role in BPD transport and BPD-PDT resistance. Furthermore, we introduce porphyrin-lipid nanovesicles as a new strategy to escape P-gp and ABCG2-mediated efflux of BPD for improved PDT outcomes in two breast cancer cell lines.

1. Introduction

One of the major problems encountered in cancer treatment is the development of multidrug resistance, a process mediated by the ATP-binding cassette (ABC) transmembrane transporters that utilize energy from ATP hydrolysis to actively pump anti-cancer agents and pro-tumorigenic molecules out of cells [1]. Among the 48 human ABC transporters identified, multidrug resistance protein 1 (MDR1, also known as P-glycoprotein or P-gp; encoded by *ABCB1*), breast cancer resistance protein (BCRP; encoded by *ABCG2*), and multidrug resistance-associated protein 1 (MRP1, encoded by *ABCC1*) are known to export hundreds of chemically unrelated anti-cancer compounds [2–4]. Over the past 30 years, the focus on developing transporter inhibitors to reverse multidrug resistance has provided little to no benefits to cancer patients [5,6]. Some transporter inhibitors are simply too toxic, while others induce pharmacokinetic changes owing to drug-drug interactions [7]. In addition, different ABC transporters are co-expressed in tumors and show high interpatient and intertumor variability with only a subset of resistant cancers expressing these transporters [6,8]. With new analytical, optical, and nanotechnology tools being developed for advancing personalized medicine, there is a surge of research interest towards the development of therapeutic agents that are poor substrates for these efflux transporter proteins [6]. This paradigm-shifting approach may result in the discovery of new agents that overcome ABC transporter-mediated resistance entirely.

Photodynamic therapy (PDT) is a mechanistically-distinct, cytotoxic modality that is effective on chemo- and radio-resistant tumors [9]. PDT uses near-infrared (NIR) light to excite a light-absorbing molecule called photosensitizer [10,11]. Upon activation, the photosensitizer induces the production of highly reactive molecular species (RMS; *e.g.*, $^1O_2$, H_2O_2, $O_2^{\bullet-}$, •OH) that confer toxicity to nearby targets [10,11]. PDT is used clinically as a salvage therapy to treat a wide range of cancers, including metastatic breast [12], esophageal [13], lung [14], basal cell [15], gastric [16], cervical [17], prostate [18], head and neck [19], brain [20], and pancreatic carcinoma [21,22]. Light delivery to confined areas such as the chest, abdomen, and brain can be done intra-

* Corresponding author. 8278 Paint Branch Drive, College Park, MD, 20742, USA.
E-mail address: hchuang@umd.edu (H.-C. Huang).

https://doi.org/10.1016/j.canlet.2019.04.037
Received 22 February 2019; Received in revised form 17 April 2019; Accepted 30 April 2019

Abbreviations

EDC	1-ethyl-3-(3-dimethylaminopropyl) carbodiimide
(16:0)LysoPC	1-palmitoyl-2-hydroxy-sn-glycero-3-phosphocholine
HPPH	2-(1-hexyloxyethyl)-2-devinyl pyropheophorbide-a
MTT	3-(4,5-dimethylthiazol-2-yl)-2,5-diphenyltetrazolium bromide
DMAP	4-(dimethylamino) pyridine
ABC	ATP-binding cassette
BPD	Benzoporphyrin derivative
BSA	Bovine serum albumin
BCRP; encoded by ABCG2	Breast cancer resistance protein
DMSO	Dimethyl sulfoxide
DOTAP	Dioleoyltrimethylammoniumpropane
DPPC	Dipalmitoylphosphatidylcholine
DSPE-PEG	Distearoylphosphatidylethanolamine-methoxy polyethylene glycol
EMEM	Eagle's minimum essential medium
FACS	Fluorescence-activated cell sorting
FBS	Fetal bovine serum
FTC	Fumitremorgin C
IC_{50}	Half maximal inhibitory concentration
MRP1	Multidrug resistance-associated protein 1
DIPEA	N,N-diisopropylethylamine
L-LysoPC-BPD	Nanoliposomal (16:0)Lyso-BPD
L-BPD	Nanoliposomal BPD
NIH	National Institutes of Health
NIR	Near-infrared
P-gp	P-glycoprotein (also known as Multidrug Resistance Protein 1, MDR1)
PBS	Phosphate-buffered saline
PDT	Photodynamic therapy
PdI	Polydispersity index
PVDF	Polyvinylidene difluoride
PpIX	Protoporphyrin IX
RMS	Reactive molecular species
TKI	Tyrosine kinase inhibitor
FDA	U.S. Food and Drug Administration

operatively or laparoscopically [22–25]. Cytotoxicity from PDT is governed by intracellular photosensitizer accumulation, subcellular localization of the photosensitizer, spatial confinement of light, and the short distances over which the RMS remain active [9–11]. Combination of targeted delivery of photosensitizer and confined light exposure often lead to a significant improvement in therapeutic efficacy [26,27]. It is well established that ABCG2 expression can limit the intracellular retention of a number of clinically used photosensitizing agents, *i.e.*, the benzoporphyrin derivative (BPD), chlorin-based drugs, aminolevulinic acid (ALA)-induced protoporphyrin IX (PpIX), as well as 2-(1-hexyloxyethyl)-2-devinyl pyropheophorbide-a (HPPH) [28]. While it has been confirmed that chlorin e6, PpIX, and HPPH are not substrates for P-gp and MRP1 [28], the role of P-gp and MRP1 in BPD transport remains unclear.

Since the discovery of P-gp over four decades ago in drug resistant cells [29–31], a number of strategies have been explored to target ABC transporters and overcome PDT resistance. Ample preclinical studies have shown that using tyrosine kinase inhibitors (TKIs; *e.g.*, imatinib mesylate, gefitinib, and erlotinib) to block drug efflux by ABC transporters could augment photosensitizer retention in cancer cells and increase PDT cytotoxicity [32–35]. Studies by Sun et al. provide evidence that gefitinib could decrease the mRNA and protein expression of ABCG2, thereby enhancing intracellular PpIX levels in a dose-dependent manner, yielding superior PDT toxicity against human glioma cell lines [33]. However, oral administration of gefitinib at 100 mg/kg was not adequate to inhibit the activity of ABCG2 in a xenograft model. This is possibly due to suboptimal experimental conditions, as well as PpIX's high affinity to human ABCG2 [32]. Using endothelial cells, Gallagher-Colombo et al. show that pretreatment with erlotinib, a potent ABCG2 inhibitor, significantly increases the intracellular BPD level and the cytotoxic effect of PDT [34]. Liu et al. suggest that imatinib mesylate increased accumulation of HPPH, PpIX, and BPD in ABCG2-overexpressing cancer cells (*i.e.*, Colo 26, RIF-1, BCC-1), but not in ABCG2 negative cells, and enhanced PDT efficacy *in vitro* [35]. A combination of imatinib mesylate and HPPH-PDT prolonged the survival of C3H/HeJCr mice bearing RIF-1 tumors compared to monotherapies. Despite convincing laboratory data showing that photosensitizer transport can be inhibited by TKIs, the clinical translatability of the TKI approach has yet to be confirmed.

As it is still unclear whether FDA-approved BPD is a substrate of P-gp and MRP1 or is a substrate of neither, we investigated the effect of P-gp and MRP1 on the intracellular accumulation of BPD in human breast cancer cell lines. Our results suggest that P-gp, like ABCG2, impairs the effectiveness of PDT in breast cancer cells by decreasing intracellular levels of BPD. While continued efforts are needed to analyze the structure-activity relationships between photosensitizers and ABC transporters, several studies indicate that the variation in photosensitizer transport correlates with the chemical structure of the photosensitizer [28,36]. Thus, we hypothesize that a tetrapyrrole-type photosensitizer with a more complex biomolecular structure will be less effectively effluxed by a variety of ABC transporters. Here, we introduce a TKI-free lipidation strategy—by conjugating photosensitizer (BPD) to lysophosphocholine (16:0)LysoPC—to escape ABCG2-and P-gp-mediated photosensitizer efflux in cancer cells. The ability of (16:0)LysoPC-BPD assemblies and its nanoformulation to improve the effectiveness of PDT is also examined in two human breast cancer cell lines.

2. Materials and methods

2.1. Cell culture

Four human breast cancer cell lines including the MCF-7 parental cell line, P-gp-overexpressing MCF-7 TX400 subline (selected in 400 ng/ml paclitaxel), ABCG2-overexpressing MCF-7 MX100 subline (selected in 100 nM mitoxantrone), and MRP1-overexpressing MCF-7/VP subline (selected in 4 μM etoposide) were maintained in Eagle's Minimum Essential Medium (EMEM) growth medium (Cellgro) supplemented with 10% (v/v) fetal bovine serum (FBS; Gibco), 100 U/mL penicillin and 100 μg/mL streptomycin (Lonza), and 0.01 mg/ml insulin (Sigma). All cell lines were characterized previously [28,36], confirmed to be free of mycoplasma, and cultured in 5% CO_2 and at 37 °C.

2.2. Western blot

Protein expression was analyzed using western blots. Briefly, 20 μg of cell lysates were separated on 4–12% precast Bis-Tris protein gels (NuPage) and transferred onto polyvinylidene difluoride (PVDF) membranes (Thermo Fisher). After blocking with 5% bovine serum albumin (BSA)-containing tris-buffered saline and Polysorbate 20 solution, proteins were detected using antibodies against ABCG2 (1:500, Kamiya BioMedical MC-177), MRP1 (1:500, Kamiya BioMedical MC-162), and P-gp (1:500, ThermoFisher MA1-26528). Anti β-actin antibodies (1:5000, Cell Signaling 3700) were used for loading control. Visualization of protein bands was developed by chemiluminescence (SuperSignal, ThermoFisher) with exposure to a Gel Imager (FluorChem E System, ProteinSimple).

2.3. Preparation and characterization of (16:0)LysoPC-BPD conjugates

The (16:0)LysoPC-BPD conjugate was synthesized by crosslinking the carboxylic acid group of BPD (U.S. Pharmacopeial Convention) to the hydroxyl functional group of (16:0)LysoPC via the esterification reaction. Briefly, 1-palmitoyl-2-hydroxy-sn-glycero-3-phosphocholine ((16:0)LysoPC), BPD, 1-ethyl-3-(3-dimethylaminopropyl) carbodiimide (EDC), 4-(dimethylamino) pyridine (DMAP), and N,N-diisopropylethylamine (DIPEA) were mixed in dichloromethane at a fixed molar ratio of 1:5:50:25:60 for 24 h at room temperature. Dichloromethane was removed via rotary evaporation, and the residue was subjected to Sephadex® LH-20 gel chromatography column purification in methanol, following which methanol was removed via rotary evaporation and the purified (16:0)LysoPC-BPD was stored at −20 °C. The purified (16:0) LysoPC-BPD conjugates were analyzed using matrix-assisted laser desorption ionization-time of flight mass spectrometry (MALDI-TOF MS; Bruker).

2.4. Synthesis and purification of nanoliposomal formulations of BPD (L-BPD) and (16:0)LysoPC-BPD (L-LysoPC-BPD)

The two types of nanoliposomes: (1) L-BPD; and (2) L-LysoPC-BPD were prepared by following our established protocol [37,38]. Briefly, dipalmitoylphosphatidylcholine (DPPC), cholesterol, distearoylphosphatidylethanolamine-methoxy polyethylene glycol (DSPE-PEG), and dioleoyltrimethylammoniumpropane (DOTAP) (Avanti Polar Lipids) were mixed in chloroform at a fixed molar ratio of 20:10:1:2.5. For the L-BPD formulation, 50 nmoles of BPD were co-dissolved with lipids at BPD-to-total lipid ratio of ~0.6 mol%. For L-LysoPC-BPD formulation, 50 nmoles of (16:0)LysoPC-BPD was co-dissolved with lipids. Chloroform was removed by rotary evaporation overnight to generate a thin lipid film. The resulting lipid film was rehydrated with 1 mL of phosphate-buffered saline (PBS) at 45 °C, and then subjected to freeze-thaw cycles (4°C-45 °C) for 2 h. The dispersion was then extruded ten times through two stacked polycarbonate membranes (0.1 μm pore size; Nuclepore, Whatman) at 45 °C using a mini-extruder system (Avanti Polar Lipids) to form unilamellar vesicles. Un-encapsulated photosensitizers or drugs were removed by dialysis (Spectra/Por, MWCO 300kD, Spectrum Laboratories) against PBS. Zetasizer NanoZS (Malvern Instruments) was used to measure the size of nanoliposomes. Concentration of BPD was determined by UV–Vis spectroscopy with an appropriate standard curve (ε = 34,895 M^{-1} cm^{-1}, at 687 nm in dimethyl sulfoxide, DMSO).

2.5. Flow cytometry

Flow cytometry studies were performed by adapting the procedure described previously [28,36]. Briefly, cells (MCF-7, MCF-7 MX100, MCF-7/VP, or MCF-7 TX400; 300k *per* 35-mm dish) were incubated with desired photosensitizing agents (*i.e.*, free BPD, (16:0)LysoPC-BPD, L-BPD or L-LysoPC-BPD; 0.25 and 1 μM) or known ABC transporter substrates (BODIPY-prazosin, Calcein AM, or Rhodamine 123; Table S1) for 1 h at 37 °C in 5% CO_2. Subsequently, cells were washed with cold PBS and then incubated with photosensitizer-free complete medium with or without known ABC transporter inhibitors (Fumitremorgin C or FTC, MK571, or valspodar; Table S1) for 1 h at 37 °C. Trypsinized cells were subsequently washed with cold PBS prior to flow cytometry analyses. Functional ABCG2 expression was confirmed by incubating MCF-7 MX100 cells in 0.25 μM BODIPY-prazosin with or without 10 μM ABCG2 inhibitor FTC. Functional MRP1 expression was determined by incubating MCF-7/VP cells in 3 μg/mL calcein-AM with or without 25 μM MRP1 inhibitor MK571. Functional P-gp was confirmed by incubating MCF-7 TX400 cells in 1 μg/ml Rhodamine 123 with or without 3 μg/mL of the P-gp inhibitor valspodar (Table S1). Samples were analyzed on a fluorescence-activated cell sorting (FACS) flow cytometer (BD FACScanto II). Calcein (Ex/Em: 494/517 nm) and Rhodamine 123 (Ex/Em: 488/515 nm) fluorescence were detected with a 488 nm laser and an AmCyan filter (525/50 nm). BODIPY-prazosin (Ex/Em: 503/512 nm) was detected using a 488 nm laser and a FITC filter (530/30 nm). BPD (Ex/Em: 435/690 nm) fluorescence was detected with a 405 nm laser and a PerCP-Cy5-5 filter (LP670 nm). At least 50,000 events were collected for all of the flow cytometry studies. The gated single cell populations were analyzed using Flowjo V10.

2.6. Photodynamic therapy (PDT) of MCF-7 parental and sub lines

Cells cultured overnight in 35-mm Petri dishes (300k cells *per* dish) were incubated with photosensitizing agents (*i.e.*, free BPD or (16:0) LysoPC-BPD; 0.25 μM) for 4 h. Subsequently, cells were washed three times with PBS and then incubated with photosensitizer-free complete medium for different periods of time (1, 16, or 24 h) prior to light activation. Photosensitizer uptake in cancer cells was determined using extraction methods as described previously [26]. PDT was performed by exposing the cells to near-infrared light (690 nm, 0–20 J/cm^2, 10 W/cm^2, bottom illumination; Modulight). Cell viability was determined by MTT [3-(4,5-dimethylthiazol-2-yl)-2,5-diphenyltetrazolium bromide] assay at 24 h after PDT following the vendor's protocol.

3. Results

3.1. BPD is an ABCG2-and P-gp-specific substrate

To determine the effects of ABC transporters on the intracellular retention of BPD photosensitizers, efflux studies were performed on a panel of human breast cancer cell lines overexpressing ABCG2, MRP1, or P-gp. Immunoblotting was used to verify high levels of ABCG2, MRP1, and P-gp in MCF-7 MX100, MCF-7/VP, and MCF-7 TX400 cell lines, respectively, compared to their parental MCF-7 cell line (Fig. 1). Cells were incubated with BPD photosensitizers or known substrates of ABC transporters (0.25 μM BODIPY-prazosin for ABCG2; 3 μg/mL Calcein AM for MRP1; 1 μg/mL Rhodamine 123 for P-gp; Table S1) for 1 h, washed with PBS, then incubated for 1 h in photosensitizer-free or substrate-free media with or without known transporter inhibitors (10 μM FTC for ABCG2; 25 μM MK571 for MRP1; 3 μg/mL valspodar for P-gp; Table S1). The intracellular fluorescence of photosensitizers or substrates were determined by flow cytometry. In ABCG2-overexpressing MCF-7 MX100 cells, the addition of ABCG2 inhibitor FTC increased both the intracellular fluorescence of BPD (Fig. 2A) and ABCG2 substrate BODIPY-prazosin (Fig. S2A). When MRP1-overexpressing MCF-7/VP cells were incubated in medium containing MRP1 substrate calcein AM with or without MRP1 inhibitor MK571, high

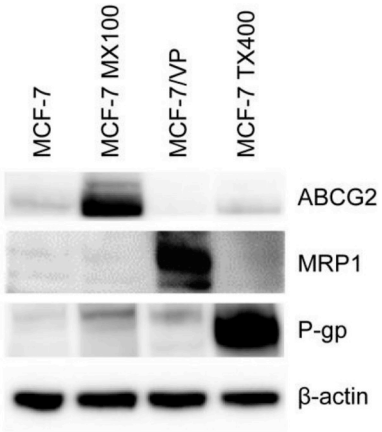

Fig. 1. Western blot analysis of ABCG2, MRP1, and P-gp expression in MCF-7, MCF-7 MX100, MCF-7/VP, and MCF-7 TX400 cells. β-Actin was used as a loading control. Whole cell extracts (20 μg) were loaded in each lane.

levels of MK571-inhibitable calcein AM efflux were observed (Fig. S2B). However, when MCF-7/VP cells were incubated with BPD in the presence or absence of MK571, no change in the intracellular levels of BPD was observed (Fig. 2B). The P-gp-overexpressing MCF-TX400 cells demonstrated high levels of valspodar-inhibitable BPD efflux (Fig. 2C) and valspodar-inhibitable Rhodamine 123 efflux (Fig. S2C). In the MCF-7 parent cell line, FTC-inhibitable BPD efflux, MK571-inhibitable BPD efflux, and valspodar-inhibitable BPD efflux were not detected

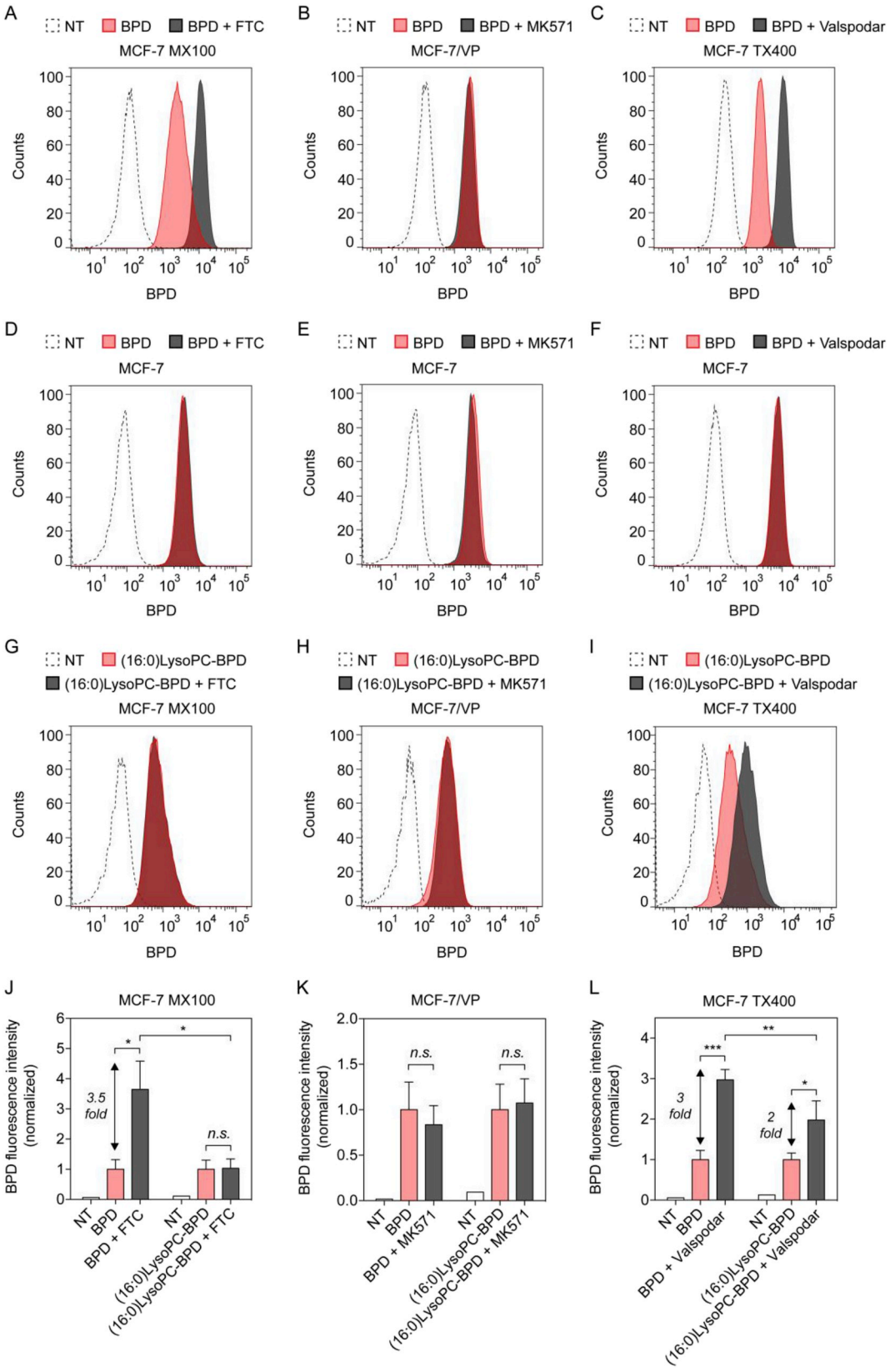

(caption on next page)

Fig. 2. BPD is transported by ABCG2 and P-gp, but not MRP1. Selected cell lines overexpressing (**A**) ABCG2 (MCF-7 MX100), (**B**) MRP1 (MCF-7/VP), or (**C**) P-gp (MCF-7 TX400), and (**D–F**) parental MCF-7 cells were incubated with 0.25 μM BPD for 1 h at 37 °C. Subsequently, cells were washed and incubated in BPD-free complete medium with or without the desired inhibitor (10 μM FTC for ABCG2, 25 μM MK571 for MRP1, or 3 μg/ml valspodar for P-gp) for 1 h at 37 °C. Intracellular fluorescence of BPD was determined using a flow cytometer equipped with the appropriate filter. Representative data from at least three independent experiments are shown. NT: not treated, control. (16:0)LysoPC-BPD is not transported by ABCG2 and MRP1, and becomes a weaker substrate of P-gp compared to BPD. Selected cell lines overexpressing (**G**) ABCG2 (MCF-7 MX100), (**H**) MRP1 (MCF-7/VP), or (**I**) P-gp (MCF-7 TX400) were incubated with (16:0)LysoPC-BPD for 1 h at 37 °C. Subsequently, cells were washed and incubated in (16:0)LysoPC-BPD-free complete medium with or without the desired inhibitor (10 μM FTC for ABCG2, 25 μM MK571 for MRP1, or 3 μg/ml valspodar for P-gp) for 1 h at 37 °C. Intracellular fluorescence of BPD was determined using a flow cytometer equipped with appropriate filter. (**J–L**) The mean intracellular fluorescence signal of BPD and (16:0)LysoPC-BPD with or without ABC transporter inhibitors in MCF-7 MX100, MCF-7/VP and MCF-7 TX400 cell lines. ($n = 3$, $^{*}P < 0.05$, $^{**}P < 0.01$, $^{***}P < 0.001$, *n.s.*: nonsignificant, two-tailed *t*-test). NT: not treated, control.

(Fig. 2D–F). These results suggest that BPD is a substrate of ABCG2 and P-gp, but not MRP1.

3.2. Lipidation of BPD affects the transport of BPD by ABCG2 and P-gp

Covalent conjugation or non-covalent association of photosensitizers and phospholipids is an expedient strategy to improve the photoactivity of photosensitizers under biologically relevant conditions and in clinical settings. Next, we investigated whether a more complex lipid-photosensitizer structure would be less effectively transported by ABCG2 and P-gp. The phospholipid-photosensitizer conjugate, (16:0) LysoPC-BPD, was synthesized by an esterification reaction between the carboxyl groups of BPD photosensitizer and the alcohol groups of (16:0) LysoPC phospholipids (Fig. S2 and Fig. S3). To evaluate the specificity of (16:0)LysoPC-BPD for ABCG2, MRP1, and P-gp, flow cytometry studies were performed on MCF-7 MX100, MCF-7/VP, and MCF-7 TX400 cells, respectively (Fig. 2G–L). When MCF-7 MX100 cells were incubated in (16:0)LysoPC-BPD with or without the ABCG2 inhibitor FTC, no FTC-inhibitable (16:0)LysoPC-BPD efflux was observed (Fig. 2G). Similarly, in MCF-7/VP cells incubated in (16:0)LysoPC-BPD with or without MRP1 inhibitor MK571, no MK571-inhibitable (16:0) LysoPC-BPD efflux was observed (Fig. 2H). When MCF-7/VP cells were incubated in (16:0)LysoPC-BPD with or without P-gp inhibitor valspodar, only minimal valspodar-inhibitable (16:0)LysoPC-BPD efflux was seen (Fig. 2I). This data indicates that (16:0)LysoPC-BPD is not an ABCG2 or MRP1 substrate, but remains a P-gp substrate.

We then compared the intracellular levels of BPD and (16:0)LysoPC-BPD with or without ABC transporter inhibitors in the selected cell lines (Fig. 2J–L). In MCF-7 MX100 cells, the addition of FTC resulted in an approximately 3.6 ± 0.9 fold increase in intracellular fluorescence of BPD, but no change in the intracellular fluorescence of (16:0)LysoPC-BPD was observed in the presence of FTC (Fig. 2J). In MCF-7/VP cells, the addition of MK571 did not alter the intracellular fluorescence of BPD or (16:0)LysoPC-BPD (Fig. 2K). In MCF-7 TX400 cells, the addition of valspodar resulted in a 3.0 ± 0.3 fold increase in the intracellular fluorescence of BPD. Interestingly, a significantly less pronounced 2.0 ± 0.5 fold increase in intracellular fluorescence of (16:0)LysoPC-BPD was observed in the presence of valspodar. This observation implies that (16:0)LysoPC-BPD could be a weaker P-gp substrate compared to BPD (Fig. 2L). We further confirmed that the escape of (16:0) LysoPC-BPD from P-gp and ABCG2-mediated efflux relies on the successful click chemistry coupling between (16:0)LysoPC and BPD (Fig. S4). Using mixtures of unconjugated (16:0)LysoPC and BPD, we showed that BPD remains a substrate of P-gp and ABCG2 (Fig. S4).

3.3. Design, preparation, and characterization of L-BPD and L-LysoPC-BPD

Hydrophobic BPD photosensitizers benefit from nanoliposomal formulation through an improvement in their pharmacokinetic profile and PDT efficacy in the clinic. Here, we prepared two nanoliposomal formulations stably entrapping BPD or (16:0)Lyso-BPD. Nanoliposomal BPD (L-BPD) and nanoliposomal (16:0)Lyso-BPD (L-LysoPC-BPD) (Fig. 3) were reproducibly synthesized via the freeze-thaw extrusion method as described previously [37,38]. Both L-BPD and L-LysoPC-BPD were grafted with ~3 mol% of PEG and formed in the size range of 140–150 nm with a narrow size distribution (polydispersity index, PdI ≤ 0.1) (Fig. 3A). The entrapment efficiency and the loading capacity of BPD or (16:0)Lyso-BPD in the nanoliposomes were determined by UV–visible spectroscopy after complete dissolution of the nanoliposomes in DMSO (Fig. 3B). Conjugation of BPD to (16:0)LysoPC did not alter the Q band (690 nm) or the Soret peak (435 nm) of BPD, as lipidation does not reduce the number of double bonds in the pyrrole rings of BPD (Fig. 3B) [39]. For L-BPD, BPD molecules were embedded within the liposomal lipid-bilayer via hydrophobic and ionic interactions at an entrapment efficiency of 78.4 ± 0.8%. In the case of L-LysoPC-BPD, BPD was covalently anchored onto (16:0)LysoPC, which serves as a lipid component in the liposome formation with entrapment efficiency of 92.7 ± 1.5%. This corresponded to approximately 267 ± 14 BPD molecules *per* liposome for L-BPD, and 273 ± 5 (16:0) LysoPC-BPD molecules *per* liposome for L-LysoPC-BPD. The liposomal formulation facilitated the monomerization of the photosensitizers and maintained the fluorescence emission signal of BPD molecules in physiologically relevant environments (Fig. 3C).

3.4. Porphyrin-lipid nanovesicle L-LysoPC-BPD escapes efflux by P-gp and ABCG2

As little data is available on the impact of nanoliposomal formulation on the efflux of photosensitizers, we next compared BPD efflux using L-BPD and L-LysoPC-BPD nanoformulations in the selected cell

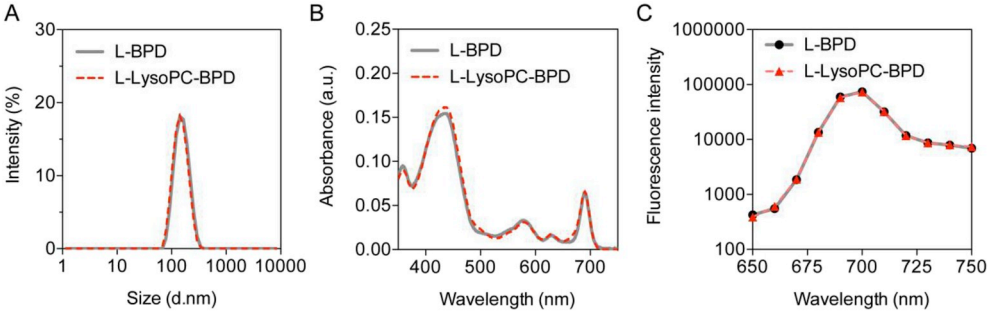

Fig. 3. Photophysical characterization of nanoliposomal BPD (L-BPD) and nanoliposomal (16:0)LysoPC-BPD (L-LysoPC-BPD). (**A**) Nanoliposomes synthesized via bilayer encapsulation BPD or (16:0)LysoPC-BPD resulted in formation of monodispersed nanoliposomes around 150 nm (PdI ≤ 0.1) and 140 nm (PdI < 0.1) respectively ($n = 3$). (**B**) Representative absorbance spectra of L-BPD and L-LysoPC-BPD in DMSO. Q band of BPD (690 nm, wavelength for light activation) was not altered in either nano-formulation. (**C**) Fluorescence spectra of L-BPD and L-LysoPC-BPD in phosphate-buffered saline.

lines (Fig. 4). In MCF-7 MX100 cells overexpressing ABCG2, incubation of FTC increased the intracellular fluorescence of L-BPD by 5.3 ± 1.3 fold (Fig. 4A); however, no significant change in the intracellular fluorescence of L-LysoPC-BPD was observed in the presence of FTC (Fig. 4B and C). In MCF-7/VP cells overexpressing MRP1, the addition of MK571 did not alter the intracellular fluorescence of L-BPD (Fig. 4D) or L-LysoPC-BPD (Fig. 4E and F). In MCF-7 TX400 cells overexpressing P-gp, the addition of valspodar led to a 3.0 ± 1.3-fold increase in intracellular fluorescence of L-BPD (Fig. 4G). On the other hand, only a modest 1.6 ± 0.1-fold increase in the intracellular fluorescence of L-

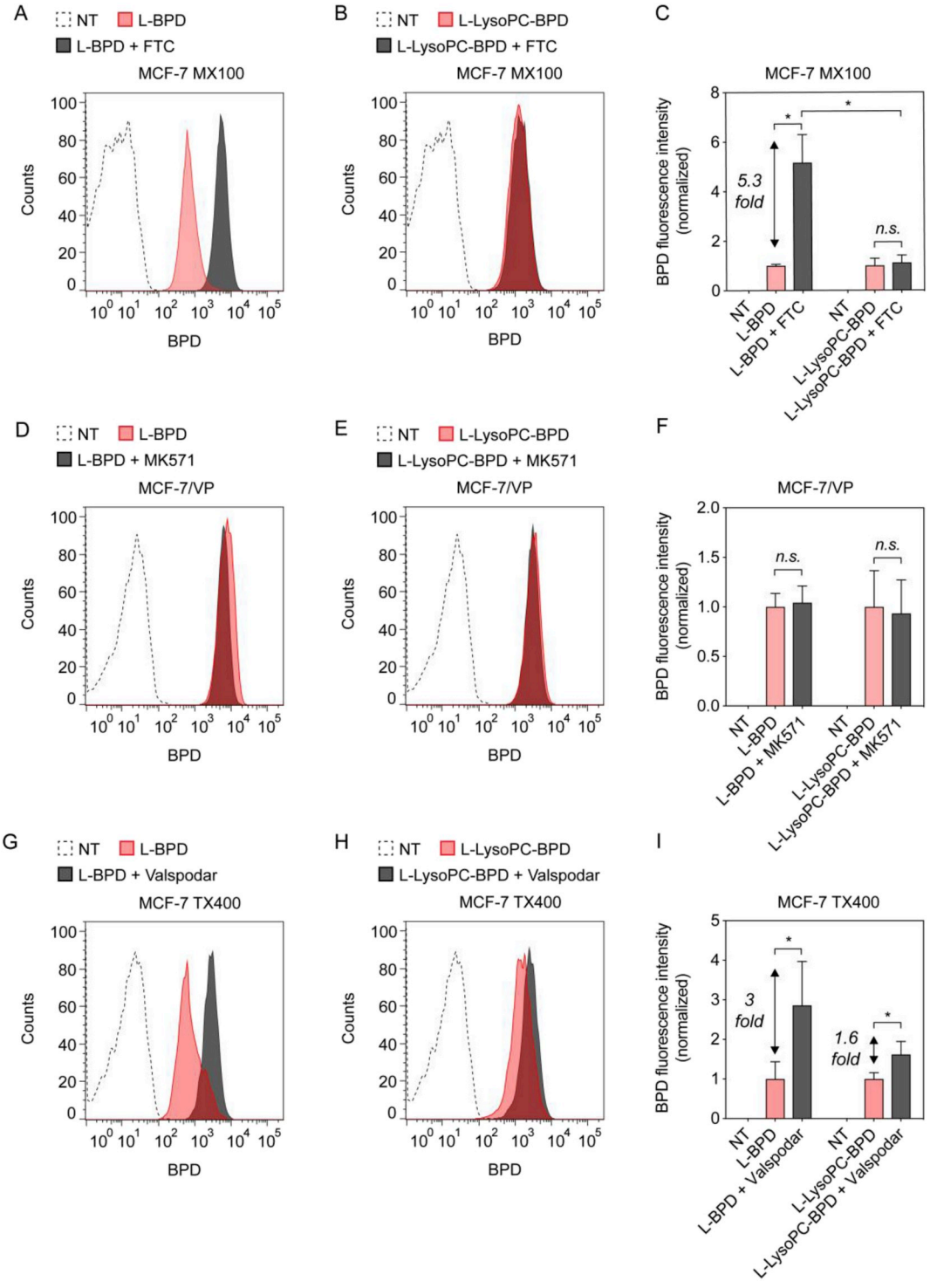

Fig. 4. Transport of nanoliposomal BPD (L-BPD) and nanoliposomal (16:0)LysoPC-BPD (L-LysoPC-BPD) by breast cancer cell lines overexpressing (**A–C**) ABCG2 (MCF-7 MX100), (**D–F**) MRP1 (MCF-7/VP), or (**G–I**) P-gp (MCF-7 TX400). Cells were incubated with 1 μM L-BPD or L-LysoPC-BPD for 1 h at 37 °C. Subsequently, cells were washed and incubated in BPD-free complete medium with or without the desired inhibitor (10 μM FTC for ABCG2, 25 μM MK571 for MRP1, or 3 μg/ml valspodar for P-gp) for 1 h at 37 °C. Intracellular fluorescence of BPD or (16:0)LysoPC-BPD were determined using a flow cytometer equipped with the appropriate filter. (**A**, **B**, **D**, **E**, **G**, **H**) Representative data are shown. The mean intracellular fluorescence signal of BPD and (16:0)LysoPC-BPD with or without ABC transporter inhibitors in (**C**) MCF-7 MX100, (**F**) MCF-7/VP, and (**I**) MCF-7 TX400 cell lines. NT: not treated, control. ($n = 3$, $^{*}P < 0.05$, $^{**}P < 0.01$, $^{***}P < 0.001$, *n.s.*: nonsignificant, two-tailed *t*-test).

LysoPC-BPD was observed in the presence of valspodar (Fig. 4H and I). We observed that although L-LysoPC-BPD evades efflux by ABCG2, it only partially evades P-gp.

3.5. L-LysoPC-BPD overcomes ABCG2 and P-gp-mediated PDT resistance

The flow cytometry studies above revealed that BPD is a substrate for P-gp and ABCG2, whereas (16:0)LysoPC-BPD is no longer a substrate for ABCG2 and becomes a weaker substrate for P-gp. We subsequently quantified the longitudinal accumulation of BPD and (16:0) LysoPC-BPD photosensitizers in MCF-7 MX100 cells expressing ABCG2 and MCF-7 TX400 cells expressing P-gp to study ABCG2-mediated and P-gp-mediated PDT resistance. In MCF-7 MX100 cells treated with BPD, we observed a dramatic 97% decrease in intracellular BPD concentration from 57.9 ± 6.8 fmoles of BPD *per* mg of protein (fmole/mg) at 1 h post-incubation, to 3.6 ± 0.6 and 1.6 ± 0.6 fmol/mg at 16 and 24 h post-incubation, respectively (Fig. 5A). In contrast, the intracellular level of (16:0)LysoPC-BPD was maintained at 13.4 ± 6.8 fmol/mg for up to 24 h in MCF-7 MX100 cells (Fig. 5A). Similarly, up to 98% reduction of intracellular BPD concentration to 2.0 ± 0.9 fmol/mg was seen in MCF-7 TX400 cells at 24 h (Fig. 5B). The intracellular (16:0)LysoPC-BPD level was maintained for up to 16 h at 10.3 ± 1.0 fmol/mg for up to 16 h in MCF-7 TX400 cells (Fig. 5B). In both MCF-7 MX100 and MCF-7 TX400 cell lines, the intracellular levels of (16:0)LysoPC-BPD were significantly higher than that of BPD at 16 and 24 h post-incubation (Fig. 5A and B).

To determine if the improved retention of (16:0)LysoPC-BPD in cancer cells would result in an enhanced PDT outcome, we performed cytotoxicity assays on MCF-7 MX100 and MCF-7 TX400 treated with (16:0)LysoPC-BPD, free BPD, or their liposomal formulations at 24 h after light irradiation (Fig. 5C and D). Both MCF-7 MX100 and MCF-7 TX400 cell lines showed resistance to PDT using BPD and L-BPD with less than 20% killing at light fluences of 5, 10 and 20 J/cm^2. Resistance to PDT was abrogated when using (16:0)LysoPC-BPD or L-LysoPC-BPD at the same incubation conditions. In MCF-7 MX100 and MCF-7 TX400 cell lines, a light-dose dependent reduction of cell viability by approximately 40%, 50%, and 70% was observed at 5, 10, and 20 J/cm^2, respectively. The half maximal inhibitory concentration (IC_{50}) values for MCF-7 MX100 and MCF-7 TX400 cells were determined to be similar at ~2.5 μM × J/cm^2 for (16:0)LysoPC-BPD and ~5 μM × J/cm^2 for L-LysoPC-BPD. The higher IC_{50} value for L-LysoPC-BPD in comparison to the IC_{50} value for (16:0)LysoPC-BPD is presumably due to the stealth properties of PEG (~3 mol%) grafted on L-LysoPC-BPD that limits photosensitizer uptake [40]. We did not determine the IC_{50} of BPD and L-BPD in MCF-7 MX100 and MCF-7 TX400 cells, due to their strong resistance to PDT and minimal cell killing.

4. Discussion

Benzoporphyrin derivative (BPD) liposome injection (Visudyne®) has been approved by the U.S. Food and Drug Administration (FDA) for the treatment of patients with wet (neovascular/exudative) age-related macular degeneration [41], and it is currently being tested in a Phase II clinical trial for PDT of metastatic breast cancer for which curative treatments are unavailable (NCT02939274). Data from The Cancer Genome Atlas (TCGA) database indicate that multiple ABC transporters (*i.e.*, ABCG2 and P-gp) are co-expressed in breast tumors and several other cancer types [6]. It has been shown that there is a positive correlation with the number of co-expressed ABC transporters and reduced relapse-free survival time in cancer patients [8]. Unfortunately, the lack of clinical success with small-molecule ABC transporter inhibitors over the past 40 years has led to a serious setback for the field [6]. This is a testimony to the desperate need for a conceptual shift to a new strategy that has the potential to overcome multidrug resistance in cancer cells. This study demonstrates that phospholipid-conjugated photosensitizing drugs can escape efflux by multiple ABC transporters and might be a way to circumvent PDT resistance.

We first examined the effect of ABCG2, P-gp, or MRP1 expression on the efflux of BPD photosensitizer using a panel of well-characterized breast cancer cell lines. The selective ABCG2 inhibitor (FTC) and P-gp inhibitor (valspodar) increased the intracellular fluorescence of BPD in cancer cells overexpressing ABCG2 and P-gp, respectively. On the other hand, in the presence of an MRP1 inhibitor (MK571), cells expressing high levels of MRP1 did not show increased intracellular fluorescence of

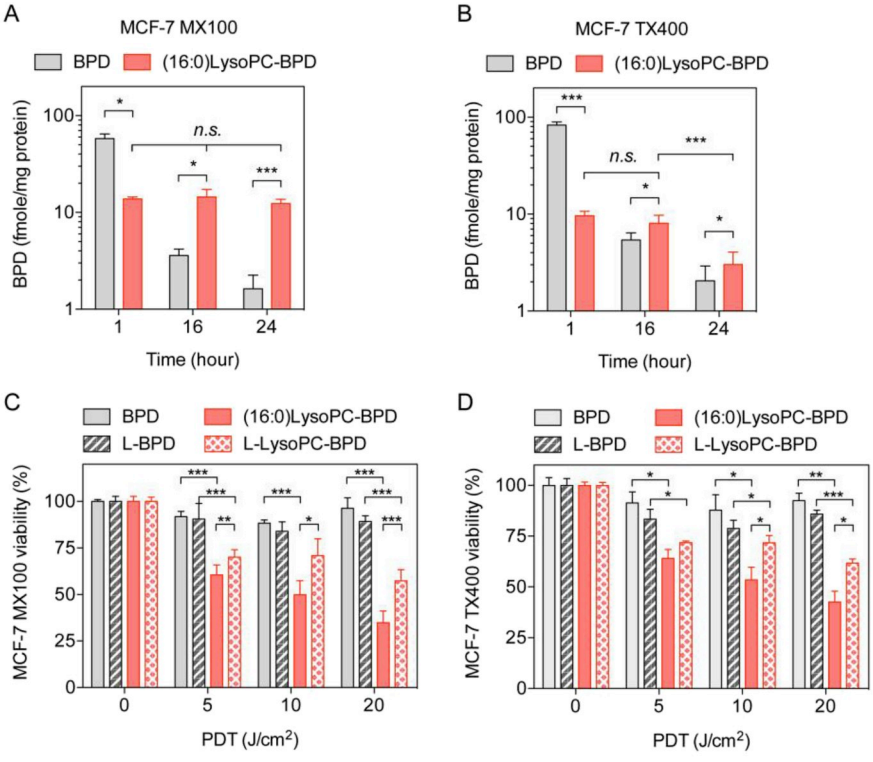

Fig. 5. Photosensitizer efflux and resistance to photodynamic therapy (PDT) were mitigated when using (16:0)LysoPC-BPD and its nanoliposomal formulation (L-LysoPC-BPD). Selected cell lines overexpressing (**A**) ABCG2 (MCF-7 MX100), or (**B**) P-gp (MCF-7 TX400) were incubated with 1 μM BPD or (16:0)LysoPC-BPD for 4 h at 37 °C. Subsequently, cells were washed and incubated in fresh medium to allow for photosensitizer efflux for 1, 16, or 24 h at 37 °C. Intracellular BPD concentration was determined using extraction methods with appropriate standard curves. Cytotoxicity assays were performed as described in the Materials and Methods section with BPD, L-BPD, (16:0)LysoPC-BPD, and L-LysoPC-BPD on (**C**) MCF-7 MX100 cells or (**D**) MCF-7 TX400 cells. (n = 3, $^*P < 0.05$, $^{**}P < 0.01$, $^{***}P < 0.001$, *n.s.*: non-significant, two-tailed *t*-test).

BPD, as measured by flow cytometry. While our observation that BPD is an ABCG2 substrate agrees with previous findings [34,35,38], this study provides new knowledge that BPD is indeed a P-gp substrate, but not an MRP1 substrate.

Visudyne® is a lyophilized mixture composed of BPD, unsaturated egg phosphatidylglycerol, and dimyristoyl phosphatidyl choline, which needs to be reconstituted with aqueous buffer to form polydispersed liposomal vesicles of BPD (200 nm–1 μm in diameter) prior to administration [42]. Based on this information, we compared the effect of ABCG2, P-gp, or MRP1 expression on the efflux of 'phospholipid-mixed' BPD and our 'phospholipid-conjugated' BPD. We show that simply mixing phospholipids and BPD does not mitigate the efflux of BPD by ABCG2 and P-gp in breast cancer cells. In contrast, covalent conjugation of phospholipid was necessary to evade the ABCG2-and P-gp-mediated transport of the phospholipid-BPD conjugates, verifying our hypothesis that photosensitizers with a more complex biomolecular structure will be effluxed in a less effective manner by a variety of ABC transporters. Our findings are in agreement with the study by Liu et al. showing that attachment of galactose to HPPH also reduced the HPPH efflux by ~50% in the RIF-1 murine radiation-induced fibrosarcoma cell line [35]. Discovery and development of bioconjugation-based photosensitizers that are poor substrates for ABC efflux pumps remains an understudied area that should be further explored.

Monodispersed nanoscopic liposomes (*i.e.*, 100–200 nm) have proven to be valuable and flexible photosensitizer delivery vehicles that allow light-triggered release of enclosed materials that home in or accumulate at desired sites preferentially to reduce the side effects of the treatment [27,43]. Nanoliposomal delivery of 'unconjugated, free-form' porphyrins and phthalocyanines to tumors was first demonstrated by Jori et al. in the 80–90's [44–46]. Pioneered by Zheng, Lovell, and colleagues, porphysomes are nanoliposomes containing 'lipid-anchored' porphyrins that can be light activated for *in vivo* photothermal or photodynamic tumor ablation [47–49]. Recognizing these advances, we develop monodispersed nanoliposomes (PdI ≤ 0.1) containing 'unconjugated, free-form' BPD, or 'lipid-anchored' BPD and compare their transport by ABCG2 and P-gp in cancer cells. Nanoliposomes containing 'lipid-anchored' BPD (*i.e.*, porphysomes) evaded photosensitizer efflux by ABCG2 and P-gp in breast cancer cells, and maintained BPD concentration in cells for at least 24 h post-incubation for effective PDT outcomes. On the other hand, 'unconjugated, free-form' BPD in nanoliposomes remained a substrate of ABCG2 and P-gp. Similarly, up to 98% of the intracellular BPD was removed from ABCG2-and P-gp-overexpressing cells at 24 h post-incubation, resulting in pronounced resistance to PDT.

In addition to PDT of cancer cells, the fluorescence signal generated from the relaxation of excited-state photosensitizers can be used for fluorescence imaging and image-guided resection of disseminated tumors [26,50]. Our data indicates that, in tumors expressing ABCG2 and P-gp, intracellular photosensitizers levels could be maintained when using 'lipid-anchored' BPD and its liposomal formation. Thus, fluorescence imaging of tumors with lipid-anchored' BPD and porphysomes could potentially be more effective for tumors which express ABCG2 and P-gp, compared to using free BPD and its liposomal formation.

In conclusion, we show that BPD photosensitizers are readily transported by P-gp and ABCG2, but not MRP1. ABCG2 and P-gp protect cancer cells from PDT with BPD. Lipidation camouflages BPD to mitigate P-gp and ABCG2-mediated efflux and improves intracellular BPD retention for enhanced PDT efficiency. Porphyrin-lipid nanovesicles also overcome ABC transporter-mediated resistance to PDT in cancer cells. Further studies to confirm whether or not these formulations are indeed poor substrates for efflux pumps and whether they could improve tumor photosensitivity and imaging *in vivo* are warranted.

Author contributions and conflict of interest

The manuscript was written through the contributions of all authors. All authors have approved the final version of the manuscript. The authors declare no potential conflict of interest.

Acknowledgements and Funding

This work was supported by the National Institutes of Health [grant number R00 CA194269] and the University of Maryland start-up fund (to H–C.H.). R.W.R., S.V.A., and M.M.G. acknowledge support from the National Institutes of Health (NIH) Intramural Research Program, National Cancer Institute, Center for Cancer Research. The fluorescence-activated cell sorting (FACS) flow cytometry study was conducted with support from the BioWorkshop hosted by the Fischell Department of Bioengineering at the University of Maryland, College Park.

Appendix A. Supplementary data

Supplementary data to this article can be found online at https://doi.org/10.1016/j.canlet.2019.04.037.

References

[1] M.M. Gottesman, T. Fojo, S.E. Bates, Multidrug resistance in cancer: role of ATP-dependent transporters, Nat. Rev. Canc. 2 (2002) 48–58.
[2] A.H. Schinkel, J.W. Jonker, Mammalian drug efflux transporters of the ATP binding cassette (ABC) family: an overview, Adv. Drug Deliv. Rev. 55 (2003) 3–29.
[3] M.M. Gottesman, O. Lavi, M.D. Hall, J.P. Gillet, Toward a better understanding of the complexity of cancer drug resistance, Annu. Rev. Pharmacol. Toxicol. 56 (2016) 85–102.
[4] A. Tamaki, C. Ierano, G. Szakacs, R.W. Robey, S.E. Bates, The controversial role of ABC transporters in clinical oncology, Essays Biochem. 50 (2011) 209–232.
[5] F.J. Sharom, ABC multidrug transporters: structure, function and role in chemoresistance, Pharmacogenomics 9 (2008) 105–127.
[6] R.W. Robey, K.M. Pluchino, M.D. Hall, A.T. Fojo, S.E. Bates, M.M. Gottesman, Revisiting the role of ABC transporters in multidrug-resistant cancer, Nat. Rev. Canc. 18 (2018) 452–464.
[7] Y.H. Choi, A.M. Yu, ABC transporters in multidrug resistance and pharmacokinetics, and strategies for drug development, Curr. Pharmaceut. Des. 20 (2014) 793–807.
[8] S. Bartholomae, B. Gruhn, K.M. Debatin, M. Zimmermann, U. Creutzig, D. Reinhardt, D. Steinbach, Coexpression of multiple ABC-transporters is strongly associated with treatment response in childhood acute Myeloid Leukemia, Pediatr. Blood Canc. 63 (2016) 242–247.
[9] T.J. Dougherty, C.J. Gomer, B.W. Henderson, G. Jori, D. Kessel, M. Korbelik, J. Moan, Q. Peng, Photodynamic therapy, JNCI, J. Natl. Cancer Inst. 90 (1998) 889–905.
[10] D.E. Dolmans, D. Fukumura, R.K. Jain, Photodynamic therapy for cancer, Nat. Rev. Canc. 3 (2003) 380–387.
[11] J.P. Celli, B.Q. Spring, I. Rizvi, C.L. Evans, K.S. Samkoe, S. Verma, B.W. Pogue, T. Hasan, Imaging and photodynamic therapy: mechanisms, monitoring, and optimization, Chem. Rev. 110 (2010) 2795–2838.
[12] S.M. Banerjee, A.J. MacRobert, C.A. Mosse, B. Periera, S.G. Bown, M.R.S. Keshtgar, Photodynamic therapy: inception to application in breast cancer, Breast 31 (2017) 105–113.
[13] T. Yano, K. Hatogai, H. Morimoto, Y. Yoda, K. Kaneko, Photodynamic therapy for esophageal cancer, Ann. Transl. Med. 2 (2014) 29.
[14] C.B. Simone 2nd, J.S. Friedberg, E. Glatstein, J.P. Stevenson, D.H. Sterman, S.M. Hahn, K.A. Cengel, Photodynamic therapy for the treatment of non-small cell lung cancer, J. Thorac. Dis. 4 (2012) 63–75.
[15] C. Matei, M. Tampa, T. Poteca, G. Panea-Paunica, S.R. Georgescu, R.M. Ion, S.M. Popescu, C. Giurcaneanu, Photodynamic therapy in the treatment of basal cell carcinoma, J. Med. Life 6 (2013) 50–54.
[16] T. Oinuma, T. Nakamura, Y. Nishiwaki, Report on the national survey of photodynamic therapy (PDT) for gastric cancer in Japan (a secondary publication), Laser Ther. 25 (2016) 87–98.
[17] W. Zhang, A. Zhang, W. Sun, Y. Yue, H. Li, Efficacy and safety of photodynamic therapy for cervical intraepithelial neoplasia and human papilloma virus infection: a systematic review and meta-analysis of randomized clinical trials, Medicine 97 (2018) e10864.
[18] N. Betrouni, S. Boukris, F. Benzaghou, Vascular targeted photodynamic therapy with TOOKAD(R) Soluble (WST11) in localized prostate cancer: efficiency of automatic pre-treatment planning, Laser Med. Sci. 32 (2017) 1301–1307.
[19] M.A. Biel, Photodynamic therapy of head and neck cancers, Methods Mol. Biol. 635 (2010) 281–293.
[20] J. Akimoto, Photodynamic therapy for malignant brain tumors, Neurol. Med.-Chir. 56 (2016) 151–157.

[21] S.G. Bown, A.Z. Rogowska, D.E. Whitelaw, W.R. Lees, L.B. Lovat, P. Ripley, L. Jones, P. Wyld, A. Gillams, A.W.R. Hatfield, Photodynamic therapy for cancer of the pancreas, Gut 50 (2002) 549–557.
[22] M.T. Huggett, M. Jermyn, A. Gillams, R. Illing, S. Mosse, M. Novelli, E. Kent, S.G. Bown, T. Hasan, B.W. Pogue, S.P. Pereira, Phase I/II study of verteporfin photodynamic therapy in locally advanced pancreatic cancer, Br. J. Canc. 110 (2014) 1698–1704.
[23] S.B. Tatter, E.G. Shaw, M.L. Rosenblum, K.C. Karvelis, L. Kleinberg, J. Weingart, J.J. Olson, I.R. Crocker, S. Brem, J.L. Pearlman, J.D. Fisher, K. Carson, S.A. Grossman, An inflatable balloon catheter and liquid 125I radiation source (GliaSite Radiation Therapy System) for treatment of recurrent malignant glioma: multicenter safety and feasibility trial, J. Neurosurg. 99 (2003) 297–303.
[24] J.S. Friedberg, Radical pleurectomy and photodynamic therapy for malignant pleural mesothelioma, Ann. Cardiothorac. Surg. 1 (2012) 472–480.
[25] C.B. Simone, K.A. Cengel, Photodynamic therapy for lung cancer and malignant pleural mesothelioma, Semin. Oncol. 41 (2014) 820–830.
[26] H.C. Huang, M. Pigula, Y. Fang, T. Hasan, Immobilization of Photo-Immunoconjugates on Nanoparticles Leads to Enhanced Light-Activated Biological Effects, Small, (2018) e1800236.
[27] H.C. H, T. H, The “nano” world in photodynamic therapy austin, J. Nanomed. Nanotechnol. 2 (2014) 1020.
[28] R.W. Robey, K. Steadman, O. Polgar, S.E. Bates, ABCG2-mediated transport of photosensitizers: potential impact on photodynamic therapy, Cancer Biol. Ther. 4 (2005) 187–194.
[29] R.L. Juliano, V. Ling, A surface glycoprotein modulating drug permeability in Chinese hamster ovary cell mutants, Biochim. Biophys. Acta 455 (1976) 152–162.
[30] P. Gros, J. Croop, I. Roninson, A. Varshavsky, D.E. Housman, Isolation and characterization of DNA sequences amplified in multidrug-resistant hamster cells, Proc. Natl. Acad. Sci. U.S.A. 83 (1986) 337–341.
[31] C.J. Chen, J.E. Chin, K. Ueda, D.P. Clark, I. Pastan, M.M. Gottesman, I.B. Roninson, Internal duplication and homology with bacterial transport proteins in the mdr1 (P-glycoprotein) gene from multidrug-resistant human cells, Cell 47 (1986) 381–389.
[32] T. Ishikawa, Y. Kajimoto, Y. Inoue, Y. Ikegami, T. Kuroiwa, Critical role of ABCG2 in ALA-photodynamic diagnosis and therapy of human brain tumor, Adv. Cancer Res. 125 (2015) 197–216.
[33] W. Sun, Y. Kajimoto, H. Inoue, S. Miyatake, T. Ishikawa, T. Kuroiwa, Gefitinib enhances the efficacy of photodynamic therapy using 5-aminolevulinic acid in malignant brain tumor cells, Photodiagn. Photodyn. Ther. 10 (2013) 42–50.
[34] S.M. Gallagher-Colombo, J. Miller, K.A. Cengel, M.E. Putt, S.A. Vinogradov, T.M. Busch, Erlotinib pretreatment improves photodynamic therapy of non-small cell lung carcinoma xenografts via multiple mechanisms, Cancer Res. 75 (2015) 3118–3126.
[35] W. Liu, M.R. Baer, M.J. Bowman, P. Pera, X. Zheng, J. Morgan, R.A. Pandey, A.R. Oseroff, The tyrosine kinase inhibitor imatinib mesylate enhances the efficacy of photodynamic therapy by inhibiting ABCG2, Clin. Cancer Res. 13 (2007) 2463–2470.
[36] R.W. Robey, K. Steadman, O. Polgar, K. Morisaki, M. Blayney, P. Mistry, S.E. Bates, Pheophorbide a is a specific probe for ABCG2 function and inhibition, Cancer Res. 64 (2004) 1242–1246.
[37] H.C. Huang, I. Rizvi, J. Liu, S. Anbil, A. Kalra, H. Lee, Y. Baglo, N. Paz, D. Hayden, S. Pereira, B.W. Pogue, J. Fitzgerald, T. Hasan, Photodynamic priming mitigates chemotherapeutic selection pressures and improves drug delivery, Cancer Res. 78 (2018) 558–571.
[38] H.C. Huang, S. Mallidi, J. Liu, C.T. Chiang, Z. Mai, R. Goldschmidt, N. Ebrahim-Zadeh, I. Rizvi, T. Hasan, Photodynamic therapy synergizes with irinotecan to overcome compensatory mechanisms and improve treatment outcomes in pancreatic cancer, Cancer Res. 76 (2016) 1066–1077.
[39] H. Abrahamse, M.R. Hamblin, New photosensitizers for photodynamic therapy, Biochem. J. 473 (2016) 347–364.
[40] M.L. Immordino, F. Dosio, L. Cattel, Stealth liposomes: review of the basic science, rationale, and clinical applications, existing and potential, Int. J. Nanomed. 1 (2006) 297–315.
[41] Guidelines for using verteporfin (Visudyne) in photodynamic therapy for choroidal neovascularization due to age-related macular degeneration and other causes: update, Retina 25 (2005) 119–134.
[42] G. Obaid, W. Jin, S. Bano, D. Kessel, T. Hasan, Nanolipid formulations of benzoporphyrin derivative: exploring the dependence of nanoconstruct photophysics and photochemistry on their therapeutic index in ovarian cancer cells, Photochem. Photobiol. 95 (2019) 364–377.
[43] B.Q. Spring, R. Bryan Sears, L.Z. Zheng, Z. Mai, R. Watanabe, M.E. Sherwood, D.A. Schoenfeld, B.W. Pogue, S.P. Pereira, E. Villa, T. Hasan, A photoactivable multi-inhibitor nanoliposome for tumour control and simultaneous inhibition of treatment escape pathways, Nat. Nanotechnol. 11 (2016) 378–387.
[44] E. Reddi, C. Zhou, R. Biolo, E. Menegaldo, G. Jori, Liposome- or LDL-administered Zn (II)-phthalocyanine as a photodynamic agent for tumours. I. Pharmacokinetic properties and phototherapeutic efficiency, Br. J. Canc. 61 (1990) 407–411.
[45] F. Ricchelli, R. Biolo, E. Reddi, G. Tognon, G. Jori, Liposomes as carriers of hydrophobic photosensitizers in vivo: increased selectivity of tumor targeting, Proc. SPIE (1987) 0847.
[46] G. Jori, L. Tomio, E. Reddi, E. Rossi, L. Corti, P.L. Zorat, F. Calzavara, Preferential delivery of liposome-incorporated porphyrins to neoplastic cells in tumour-bearing rats, Br. J. Canc. 48 (1983) 307–309.
[47] J.F. Lovell, C.S. Jin, E. Huynh, H. Jin, C. Kim, J.L. Rubinstein, W.C. Chan, W. Cao, L.V. Wang, G. Zheng, Porphysome nanovesicles generated by porphyrin bilayers for use as multimodal biophotonic contrast agents, Nat. Mater. 10 (2011) 324–332.
[48] D. Miranda, J.F. Lovell, Mechanisms of light-induced liposome permeabilization, Bioeng. Transl. Med. 1 (2016) 267–276.
[49] S. Shao, J. Geng, H. Ah Yi, S. Gogia, S. Neelamegham, A. Jacobs, J.F. Lovell, Functionalization of cobalt porphyrin-phospholipid bilayers with his-tagged ligands and antigens, Nat. Chem. 7 (2015) 438–446.
[50] W. Stummer, E. Suero Molina, Fluorescence imaging/agents in tumor resection, Neurosurg. Clin. 28 (2017) 569–583.